# Continuous wave Nd:YAG channel waveguide laser produced by focused proton beam writing

**Yicun Yao,[1] Yang Tan,[1] Ningning Dong,[1] Feng Chen,[1,2,*] and Andrew A. Bettiol[3]**

*[1]School of Physics, Shandong University, Jinan 250100, China*
*[2]State Key Laboratory of Crystal Materials, Shandong University, Jinan 250100, China*
*[3]Centre for Ion Beam Applications, Department of Physics, National University of Singapore, Singapore*
*[*]drfchen@sdu.edu.cn*

**Abstract:** We report on mirrorless continuous wave laser oscillation at 1064 nm from a 808 nm pumped Nd:YAG optical channel waveguide fabricated by 1 MeV focused proton beam writing. Pump power threshold has been found to be 94 mW with a laser slope efficiency of 40%. A maximum output power at 1064 nm for the waveguide laser is 63 mW at absorbed pump power of 247 mW.

©2010 Optical Society of America

**OCIS codes:** (230.7380) Waveguides, channeled; (160.3380) Laser materials; (140.3570) Lasers, single-mode.

## References and links

1. J. I. Mackenzie, "Dielectric Solid-State Planar Waveguide Lasers: A Review," IEEE J. Sel. Top. Quantum Electron. **13**(3), 626–637 (2007).
2. G. Lifante, *Integrated Photonics: Fundamentals* (John Wiley & Sons Ltd, West Sussex, 2003).
3. G. I. Stegeman, and C. T. Seaton, "Nonlinear integrated optics," J. Appl. Phys. **58**(12), R57 (1985).
4. C. J. M. Smith, H. Benisty, S. Olivier, M. Rattier, C. Weisbuch, T. F. Krauss, R. M. De La Rue, R. Houdré, and U. Oesterle, "Low-loss channel waveguides with two-dimensional photonic crystal boundaries," Appl. Phys. Lett. **77**(18), 2813–2815 (2000).
5. F. Chen, X. L. Wang, and K. M. Wang, "Development of ion-implanted optical waveguides in optical materials: A review," Opt. Mater. **29**(11), 1523–1542 (2007).
6. E. J. Murphy, *Integrated optical circuits and components: Design and applications* (Marcel Dekker, New York, 1999).
7. F. Watt, M. B. H. Breese, A. A. Bettiol, and J. A. van Kan, "Proton beam writing," Mater. Today **10**(6), 20–29 (2007).
8. J. A. van Kan, A. A. Bettiol, and F. Watt, "Three-dimensional nanolithography using proton beam writing," Nucl. Instrum. Methods Phys. Res. B **181**, 49 (2001).
9. H. J. Whitlow, M. L. Ng, V. Auželyté, I. Maximov, L. Montelius, J. A. van Kan, A. A. Bettiol, and F. Watt, "Lithography of high spatial density biosensor structures with sub-100 nm spacing by MeV proton beam writing with minimal proximity effect," Nanotechnology **15**(1), 223–226 (2004).
10. T. C. Sum, A. A. Bettiol, C. Florea, and F. Watt, "Proton-beam writing of poly-methylmethacrylate buried channel waveguides," J. Lightwave Technol. **24**(10), 3803–3809 (2006).
11. K. Ansari, J. A. van Kan, A. A. Bettiol, and F. Watt, "Fabrication of high aspect ratio 100 nm metallic stamps for nanoimprint lithography using proton beam writing," Appl. Phys. Lett. **85**(3), 476–478 (2004).
12. A. A. Bettiol, S. Venugopal Rao, T. C. Sum, J. A. van Kan, and F. Watt, "Fabrication of optical waveguides using proton beam writing," J. Cryst. Growth **288**(1), 209–212 (2006).
13. A. A. Bettiol, T. C. Sum, F. C. Cheong, C. H. Sow, S. Venugopal Rao, J. A. van Kan, E. J. Teo, K. Ansari, and F. Watt, "A progress review of proton beam writing applications in microphotonics," Nucl. Instrum. Methods Phys. Res. B **231**(1-4), 364–371 (2005).
14. T. C. Sum, A. A. Bettiol, H. L. Seng, I. Rajta, J. A. van Kan, and F. Watt, "Proton beam writing of passive waveguides in PMMA," Nucl. Instrum. Methods Phys. Res. B **210**, 266–271 (2003).
15. T. C. Sum, A. A. Bettiol, J. A. van Kan, F. Watt, E. Y. B. Pun, and K. K. Tung, "Proton beam writing of low-loss polymer optical waveguides," Appl. Phys. Lett. **83**(9), 1707–1709 (2003).
16. A. Benayas, D. Jaque, Y. Yao, F. Chen, A. A. Bettiol, A. Rodenas, and A. K. Kar, "Micro-structuring of Nd:YAG crystals by proton beam writing," Opt. Lett. (to be published).
17. A. A. Bettiol, S. Venugopal Rao, E. J. Teo, J. A. van Kan, and F. Watt, "Fabrication of buried channel waveguides in photosensitive glass using proton beam writing," Appl. Phys. Lett. **88**(17), 171106 (2006).
18. M. Domenech, G. V. Vázquez, E. Cantelar, and G. Lifante, "Continuous-wave laser action at λ=1064.3 nm in proton- and carbon- implanted Nd:YAG waveguides," Appl. Phys. Lett. **83**(20), 4110–4112 (2003).
19. F. Chen, Y. Tan, and D. Jaque, "Ion-implanted optical channel waveguides in neodymium-doped yttrium aluminum garnet transparent ceramics for integrated laser generation," Opt. Lett. **34**(1), 28–30 (2009).

20. G. A. Torchia, P. F. Meilán, A. Rodenas, D. Jaque, C. Mendez, and L. Roso, "Femtosecond laser written surface waveguides fabricated in Nd:YAG ceramics," Opt. Express **15**(20), 13266–13271 (2007).
21. J. Siebenmorgen, K. Petermann, G. Huber, K. Rademaker, S. Nolte, and A. Tünnermann, "Femtosecond laser written stress-induced $Nd:Y_3Al_5O_{12}$ (Nd:YAG) channel waveguide laser," Appl. Phys. B **97**(2), 251–255 (2009).
22. A. Ródenas, G. A. Torchia, G. Lifante, E. Cantelar, J. Lamela, F. Jaque, L. Roso, and D. Jaque, "Refractive index change mechanisms in femtosecond laser written ceramic Nd:YAG waveguides: micro- spectroscopy experiments and beam propagation calculations," Appl. Phys. B **95**(1), 85–96 (2009).
23. G. A. Torchia, A. Rodenas, A. Benayas, E. Cantelar, L. Roso, and D. Jaque, "Highly efficient laser action in femtosecond-written Nd:yttrium aluminum garnet ceramic waveguides," Appl. Phys. Lett. **92**(11), 111103 (2008).
24. F. Watt, J. A. van Kan, I. Rajta, A. A. Bettiol, T. F. Choo, M. B. H. Breese, and T. Osipowicz, "The National University of Singapore high energy ion nano-probe facility: Performance tests," Nucl. Instrum. Methods Phys. Res. B **210**, 14–20 (2003).
25. J. F. Ziegler, computer code, SRIM *http://www.srim.org*.
26. D. Yevick, and W. Bardyszewski, "Correspondence of variational finite-difference (relaxation) and imaginary-distance propagation methods for modal analysis," Opt. Lett. **17**(5), 329–330 (1992).
27. Y. Tan, and F. Chen, "Proton-implanted optical channel waveguides in Nd:YAG laser ceramics," J. Phys. D **43**(7), 075105 (2010).

## 1. Introduction

Optical waveguides offer compact confinement of light propagation down to dimensions of a few micrometers; as a result, the optical intensities within these small volumes reach much higher levels with respect to the bulk samples. Benefiting from high intracavity intensity owing to the reduced active volumes, waveguide lasers show many advantages when compared to their bulk counterparts, such as lower threshold and higher laser slope efficiencies [1]. Those features make waveguide laser devices suitable as fundamental components in modern integrated photonic systems [2,3]. In practice, two-dimensional (2D) waveguides (typically in channel or ridge configurations) show a superior performance than one dimensional (1D) structures (i.e., planar or slab waveguides) because of the more compact geometry in 2D cases that further enhances the optical intensities achieved while reducing the cost for substrate materials [4,5]. In addition, if the physical shapes and correlated modal profiles have suitable dimensions, 2D waveguides can be easily connected with optical fibers with a high coupling efficiency for construction of integrated photonic systems [6].

Proton Beam Writing (PBW) is an advanced technique that is used for the inscription of three-dimensional (3D) structures in diverse materials [7]. PBW is based on the controlled scanning of a focused proton beam within the material to be micro-structured so that local modifications can be achieved in a precise manner at both micro- and submicron scales [8]. Because of the energy and momentum mismatch between protons and electrons in the target material, the protons will maintain a straight pathway and cause little proximity effect as energy obtained by secondary electrons will be low [9]. This makes PBW an efficient technology to fabricate 3D high aspect ratio nanostructures in various materials [10]. When compared to normal ion implantation (that requires the additional use of masks), PBW shows the intriguing advantage of direct fabrication due to the use of focused ion beams of micro- (and even sub-micron) size, realizing maskless implantation of energetic protons [10]. In recent years PBW has also shown its advantages for optical waveguide fabrication [11,12]. As of yet, successful examples of PBW waveguides include a few organics materials (e.g., PMMA, SU-8) glasses and crystals [13–17].

Neodymium doped yttrium aluminum garnet (hereafter abbreviated to Nd:YAG) is one of the most important gain media for solid state lasers owing to its outstanding fluorescence, mechanical and thermal properties. Waveguide lasers have been already fabricated in this material (in both single crystals and polycrystalline ceramics) by using a few techniques, such as ion implantation, femtosecond laser inscription, femtosecond laser ablation, film deposition, and waveguide lasers have been generated in some of these samples [18–23]. Despite the fact that PBW has been recently demonstrated to be a powerful technique for the fabrication of high quality channel waveguides in Nd:YAG with 3D control [16], the suitability of the obtained waveguides as integrated laser gain medium has not, to the best of

our knowledge, been reported up to now. In this work, we report on the first demonstration of continuous wave stable laser operation at 1064 nm at room temperature from a 808 nm pumped Nd:YAG channel waveguide fabricated by PBW.

## 2. Experiments in details

The optically polished Nd:YAG (doped by 1 at. % $Nd^{3+}$ ions) crystal used in this work was cut into dimensions of $10(x) \times 4.8(y) \times 1.5(z)$ mm$^3$. The PBW process was carried out by using the facilities at the Center for Ion Beam Applications, National University of Singapore [24]. The proton beam was at energy of 1 MeV and focused down to a beam with diameter of 1μm. During the process, the sample was mounted on a motorized stage (Exfo inchworm stage, moving linearly at different speeds), and the proton beam was magnetically scanned over a distance of 4μm in a perpendicular direction to the proton pathway on the $x$-$y$ face, reaching different writing fluences of $1 \times 10^{15}$, $5 \times 10^{15}$, $1 \times 10^{16}$, and $2 \times 10^{16}$ cm$^{-2}$. The formed channel waveguides were along the 4.8-mm axis of the wafer. Figure 1 shows the calculated defect (defect per atom, DPA) and H$^+$ concentration profiles caused by the 1 MeV proton beam in Nd:YAG, as obtained with the SRIM 2010 code [25]. As one can see, the projected average ion range ($R_p$) of the 1 MeV protons in Nd:YAG crystal is ~9.8 μm. The proton-induced damage is very low even at the barrier region (maximally of 0.012), which suggests minor modification on the original lattices of Nd:YAG. In addition, the profile of the focused proton beam is approximately Gaussian, and at 1 MeV it will have a lateral straggling of ~0.7 μm, which results in channel waveguides with a transverse width of ~4.7 μm at the cross section.
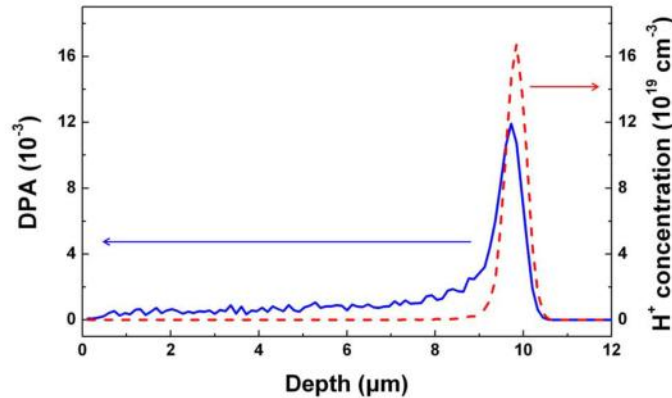


Fig. 1. The defects per atom (DPA) (blue solid line) and H$^+$ range (red dashed line) profiles of proton beam at energy of 1MeV and fluence of $1 \times 10^{16}$ cm$^{-2}$ based on SRIM calculation.

A conventional end-face coupling optical system was used to measure the modal profiles of the waveguides at wavelength of 632.8 nm by using a He-Ne laser. The 2D refractive index ($n$) profiles of the waveguides were reconstructed and the light propagation was simulated by using the finite-difference beam propagation method (FD-BPM) [26].

The confocal microphotoluminescence (μPL) spectra from both the waveguide and bulk were obtained by using a fiber-coupled confocal microscope (Olympus BX-41) as described elsewhere [21]. The 10-mW cw radiation at 488 nm from an argon laser was focused at sample's surface by using a $100 \times$ objective (numerical aperture N.A. = 0.95), exciting the $Nd^{3+}$ ions from their fundamental state ($^4I_{9/2}$) up to the excited state ($^2G_{3/2}$). The subsequent $^4F_{3/2} \rightarrow ^4I_{11/2}$ emissions were collected by using the same microscope objective and, after passing through a confocal aperture, analyzed by a CCD camera attached to a fiber-coupled spectrometer.

The laser operation experiment was performed by using end-face pumping system. A 808 nm light beam generated from a tunable Ti:sapphire cw laser (Coherent 110) was focused by a convex lens (focus length of 25mm) into the input face of the waveguide laser. The laser cavity (plane-plane geometry) was a mirror-less cavity so that optical feed-back was directly

provided by the Fresnel reflections caused by the two end-faces of the Nd:YAG crystal. Thus, since the refractive index of Nd:YAG is close to 1.8, both end-faces act as output couplers with an effective transmittance close to 0.92. The waveguide laser beam generated at ~1064 nm was collected and collimated by using a 20× microscope objective. The laser radiation at 1064 nm was discriminated from the non-absorbed pump radiation by using a dichroic mirror/filter (with transmittance of 90% at 1064 nm and reflectivity of >99% at 808 nm) from the 808-nm beam. The output laser beam was imaged by an infrared CCD camera and analyzed by a spectrometer. The laser power (from both end-faces of the crystal) was monitored by a powermeter.
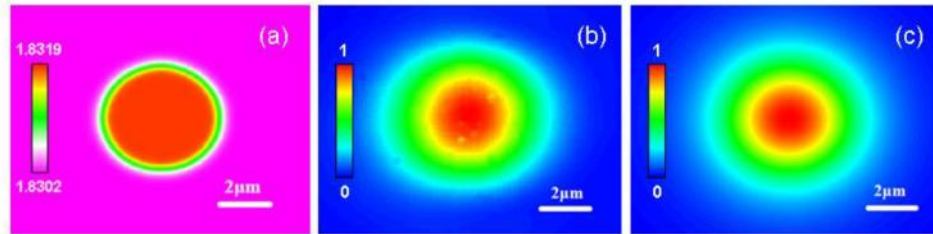
## 3. Results and discussion



Fig. 2. (a) Reconstructed index profile, (b) measured and (c) calculated modal profiles with normalized intensity of the fundamental mode corresponding to the Nd:YAG channel waveguide produced by 1MeV PBW at fluence of $1\times10^{16}$ cm$^{-2}$.

End coupling experiments at 632.8 nm show that the light was well confined in the waveguides produced by 1MeV PBW at fluences of $5\times10^{15}$, $1\times10^{16}$, and $2\times10^{16}$ cm$^{-2}$, while not guided at fluence of $1\times10^{15}$ cm$^{-2}$ (due to the very low-fluence irradiation). Figure 2(b) shows the measured near-field intensity distribution of the 632.8 nm transmitted light in the fundamental mode of the waveguide produced by PBW at fluence of $1\times10^{16}$ cm$^{-2}$. As it can be appreciated, the shape of the waveguide's mode is circular with a FWHM of 3.4 μm, which suggests a good potential match of the light field into (or from) optical fibers. More importantly, the waveguide mode is observed at about 10-μm depth as measured from the sample surface (i.e., the center of the waveguide core is located at a depth of ~9.7μm), which confirms that the waveguide exists at the end of ion range (i.e., at the so-called the nuclear damage region) [Fig. 1]. Different from the previous reports on Nd:YAG waveguides fabricated by normal ion implantation, where the optical barrier (with negative index changes, $\Delta n < 0$) has been assumed, the focused PBW constructs an enhanced well (with $\Delta n > 0$) at the nuclear damage region [18,19]. The increment is very likely a local enhancement in the electronic polarizability caused by nuclear collisions [16]. The very small size of the waveguide cross section makes it hard to measure the index distribution directly. Nevertheless, by assuming a step index profile, the change of refractive index in the PBW waveguide could be roughly estimated by measuring the N.A. of the waveguides, using the formula

$$\Delta n = \frac{\sin^2 \Theta_m}{n} \tag{1}$$

where the N.A. is the numerator of the formula right side and $\Theta_m$ of the maximum incident angular deflection at which no guiding light occurring, while $n$ the refractive index of the substrate. The $\Delta n$ change was determined to be $1.7\times10^{-3}$. By also considering the approximately centrosymmetrical geometry of the near-field profile, we reconstructed the 2D refractive index around the guiding structure as shown in Fig. 2(a). Based on this reconstructed index distribution, we calculated the modal profile [Fig. 2(c)] of waveguide by using FD-BPM with the commercial software BeamPROP©. By comparing Figs. 2(b) and

(c), one can conclude that the simulated distribution is in good agreement with the measured modal profile.
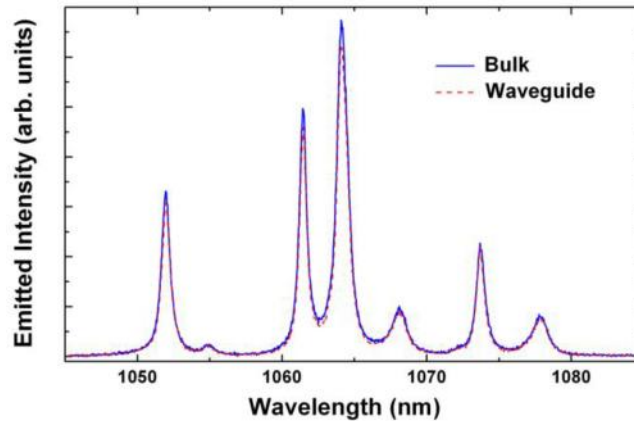


Fig. 3. Comparison of the room temperature micro-luminescence emission spectra correlated to $Nd^{3+}$ ions at $^4F_{3/2} \rightarrow ^4I_{11/2}$ transition obtained from the channel waveguide (dashed line) and the bulk (solid line).

Figure 3 shows the comparison of the $^4F_{3/2} \rightarrow ^4I_{11/2}$ room-temperature μ-PL emission spectra (intensity vs. wavelength) of $Nd^{3+}$ ions obtained from the waveguide and the bulk. As it can be observed, the fluorescence intensity and shape obtained from the waveguide are nearly the same as that obtained from the bulk (reflecting that both pumping efficiency and $^4F_{3/2}$ quantum yield of $Nd^{3+}$ ions were not strongly modified by the PBW procedure). This is in good agreement with the defect calculation (only ~1% DPA) obtained by SRIM code (Fig. 1). Data included in Fig. 3 shows that the outstanding luminescence features of $Nd^{3+}$ ions are well preserved in at waveguide's volume. This, in turn, makes the PBW Nd:YAG waveguides promising candidates for highly efficient laser light generation. From a fundamental point of view, the observed almost unaffected fluorescence efficiency reveals that the waveguide region is not accompanied by a large density of lattice defects and/or luminescence quenching centers, which is ubiquitous in Nd:YAG waveguides produced by normal ion implantation; as an example ion-induced defects leads to a overall $Nd^{3+}$ luminescence reduction close to 25% in proton implanted Nd:YAG ceramic waveguides [27].
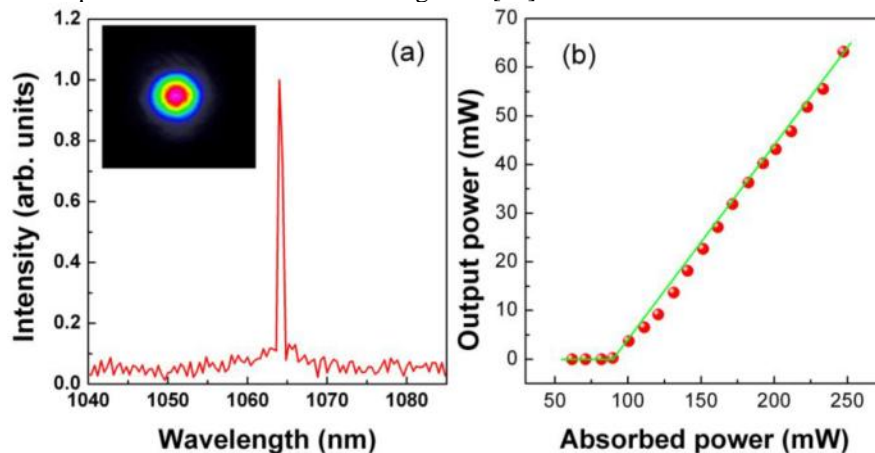


Fig. 4. (a) Laser oscillation spectra from the waveguide produced by 1 MeV PBW at fluence of $1 \times 10^{16}$ cm$^{-2}$, showing a keen-edged peak at 1064.2 nm with a FWHM of 0.75nm. The mode image of the waveguide laser is shown as inset. (b) The measured output laser power as a function of the absorbed pump power (balls) from the waveguide. The green solid line shows the linear fit of the experimental data.

Figure 4(a) depicts the laser emission spectra around 1064 nm from the 1 MeV PBW Nd:YAG waveguide at fluence of $1\times10^{16}$ cm$^{-2}$ as the absorbed pump power is above the threshold. The center wavelength of the laser spectrum is 1064.2 nm, which indeed corresponds to the strongest emission line within the ${}^4F_{3/2}\rightarrow{}^4I_{11/2}$ transition of Nd$^{3+}$ ions. The FWHM of the emission line is ~0.75 nm, clearly denoting the presence of laser oscillation. The inset shows the obtained image of the waveguide laser mode (near-field intensity distribution). The waveguide mainly shows a clear single mode character, being this outstanding feature of relevance in many practical applications.

Considering the widths of the pump beam (~16 μm) at 808 nm and the laser mode (~3.4 μm) the 1064 nm, the pump coupling efficiency is estimated to be ~40%. The absorption efficiency of the waveguide was measured to be 0.9. Figure 4(b) shows the output laser power (at 1064.2 nm) as a function of the absorbed pump power (at 808 nm) generated by the Nd:YAG waveguide at a writing fluence of $1\times10^{16}$ cm$^{-2}$. The laser power in Fig. 4(b) accounts for the laser radiations coming out from both faces of the crystal. From the linear fit of the experimental data, we have determined that the power threshold for the laser oscillation is 94 mW and that a slope coefficient of 40% can be achieved from the present waveguide laser system. This laser slope efficiency can be compared to those previously reported from other Nd:YAG mirrorless waveguide lasers. The maximum 1064-nm laser power achieved is 63 mW for the maximum absorbed pump power of 247 mW, leading to an optical conversion efficiency of 25.5%. As an example it has been found that is significantly smaller than that obtained from Ultrafast Laser Inscribed (ULI) waveguides (60%). One possible reason for this difference is the larger propagation losses of the PBW waveguides (~4 dB/cm, mainly due to the nuclear damage induced by the proton beams) in respect to those of ULI waveguides (below 1dB/cm) [16,23]. In addition, the two end-faces may not be perfectly perpendicular to the channels, which could bring out dramatic degrade of the performance of the Nd:YAG waveguide laser system. Nevertheless, by reducing the propagation loss of the waveguides by the thermal annealing and avoiding the misalignment of the channels, waveguide lasers with better performance may be expected. It is also important to remark that the PBW waveguide lasers demonstrated here show a superior mode quality (highly symmetric) in respect to ULI mirrorless waveguide lasers in Nd:YAG crystals [23].

## 4. Summary

We have reported on the fabrication of optical channel waveguides in Nd:YAG laser crystals at the nuclear-damage regions by using maskless proton beam writing. The well-defined modal profiles and the absence of any relevant deterioration in the fluorescence properties of Nd ions at waveguide's volume have suggested good guiding properties. These good perspectives have been experimentally confirmed. The cw laser has been generated at 1064 nm with a maximum output power of 63 mW under 808-nm optical pump in a mirrorless configuration. The pump threshold of 94 mW and the slope efficiency of 40% have been determined.

### Acknowledgments